JOURNAL OF PROPULSION AND POWER
Vol. 24, No. 5, September–October 2008

Shock Train Leading-Edge Detection in a Dual-Mode Scramjet

D. B. Le,* C. P. Goyne,† and R. H. Krauss‡
University of Virginia, Charlottesville, Virginia 22904

DOI: 10.2514/1.32592

Time-resolved pressure measurements in a dual-mode scramjet isolator were examined to investigate the potential for using the measurements for shock train leading-edge detection. Changes in the pressure magnitude, standard deviation levels, and frequency content were observed as the shock train advanced upstream past each pressure measurement station. Three detection criteria were defined and examined: 1) 150% of the normalized pressure magnitude upstream of combustion influences, 2) 150% of the normalized pressure standard deviation level upstream of combustion influences, and 3) the maximum value of the normalized pressure standard deviation. Another method of shock train leading-edge detection involved the examination of the frequency content of the pressure signal using power spectra analysis. Results indicated that the second detection criterion provided the earliest method of shock train detection as the shock train moved upstream, followed by the first and third criteria. Also, the frequency content of the pressure signals significantly changed near the shock train leading edge. However, a comparison of this method to the three criteria first examined showed that it did not provide earlier shock train detection.

Nomenclature

a	=	speed of sound
H	=	normal height of ramp fuel injector
M	=	Mach number
P	=	pressure
R	=	gas constant
T	=	temperature
t	=	time
X	=	scramjet axial location with origin at base of fuel injector
γ	=	specific heat ratio
σ	=	standard deviation
ϕ	=	equivalence ratio

Subscripts

max	=	maximum quantity
ref	=	reference quantity at isolator inlet
up	=	upstream of combustion influences

I. Introduction

THE dual-mode scramjet (DMSJ) is a particularly attractive hypersonic airbreathing propulsion system because it combines the operational capabilities of a ramjet and a scramjet into one flowpath [1–3]. At Mach numbers below approximately 4, the DMSJ operates in ram mode whereby combustion occurs at subsonic conditions. This is achieved by managing the heat release in the combustor such that a thermal choke is achieved and a precombustion shock train forms in the DMSJ isolator. The shock train consists of a series of normal or oblique shocks, which terminate with a normal shock that drives the flow to subsonic conditions. However, at high Mach numbers, forcing the flow to subsonic conditions results in increased pressure losses and decreased operational efficiency [3]. This can be averted by allowing the flow to remain supersonic. At a fixed Mach number, the transition from subsonic to supersonic combustion occurs by alleviating the thermal choke using flowpath geometry modification and/or control of the heat release due to combustion. During mode transition, the precombustion shock train may exist as a series of normal or oblique shocks, depending upon boundary conditions [3]. Once the thermal choke is fully alleviated, the flow through the combustor remains supersonic. In this mode of operation, combustion occurs predominantly under supersonic conditions.

The function of the isolator is to contain the shock train and prevent interaction between the scramjet combustor and the supersonic inlet. However, the length of the shock train varies depending upon operating conditions and is dependent upon factors such as isolator geometry and the combustor-to-inlet pressure ratio. During normal operation, an increase in the combustor equivalence ratio will cause the combustor-to-inlet pressure ratio to increase, and the length of the shock train will increase according to established empirical relations [1]. If the combustor-to-inlet pressure ratio becomes too large, the shock train may interact with the inlet, which would lead to inlet and engine unstart. Unstart is characterized by high thermal and pressure loads, loss of air-mass capture, and an increase in drag, which combined may result in the loss of the vehicle and/or mission failure [3]. It is thus necessary to locate the shock train and control its location in the isolator to avoid unstart.

For the purpose of preventing combustor–inlet interaction, the location of the upstream extent of the isolator shock train is of utmost importance. Depending on whether the shock train consists of a series of normal or oblique shocks, the upstream extent, or leading edge, will either be a bifurcated normal shock or an oblique shock, respectively. The nature of such shock trains have been extensively studied [4]. The turbulent nature of a boundary layer is known to be significantly altered through interaction with normal and oblique shocks and, if the boundary layer separates, the flow will be highly unsteady [5]. However, the turbulent structure of the boundary layer will significantly change even if separation does not occur [6]. For both the normal and oblique shock train, the leading-edge shock separates the boundary layer. In the case of the normal shock train, the boundary layer reattaches whereas the flow remains separated in the case of the oblique shock train [3]. Monitoring the turbulent nature and unsteadiness of the boundary layer would thus seem a reliable way to monitor the location of the shock train leading edge,

Presented as Paper 0815 at the 44th AIAA Aerospace Sciences Meeting and Exhibit, Reno, NV, 9–12 January 2006; received 3 June 2007; revision received 3 December 2007; accepted for publication 15 December 2007.

*Graduate Research Assistant, Mechanical and Aerospace Engineering; currently NASA Langley Research Center, Mail Stop 442, Hampton, VA 23602. Member AIAA.

†Research Assistant Professor, Mechanical and Aerospace Engineering, Aerospace Research Laboratory, PO Box 400248. Senior Member AIAA.

‡Research Consultant, Rammatek LLC, Aerospace Research Laboratory, PO Box 400248.

regardless of the shock train structure. One relatively easy way to monitor the boundary layer is through time-resolved wall pressure measurements. Obviously, the rise in pressure magnitude associated with the shock train would seem to be the easiest method to locate the shock train leading edge but, as will be discussed, this is not always the case for operational applications.

The potential of using time-resolved pressure measurements for shock train leading-edge detection in supersonic inlets has been investigated previously [7]. The investigators examined the axial distributions of instantaneous pressure magnitude and quantities such as broadband rms intensity and spectral content as a means of locating the leading edge of a shock train induced through (noncombustion) back pressure. The results were compared against schlieren visualization. Instantaneous pressure distributions and rms intensity monitoring located the shock train leading edge well. The investigators also artificially introduced an acoustic disturbance of known frequency downstream of the shock train and monitored the boundary layer upstream of the shock train to see if the disturbances could be used to detect the shock train leading edge. This particular method was largely unsuccessful and, overall, the investigators recommended monitoring the distributions of instantaneous pressure magnitude. However, the authors noted that this method relies on prior knowledge of the inlet performance that may include a large database. Such a database might involve variable inlet geometries and different freestream Mach numbers, pressures, and vehicle conditions (such as pitch and yaw). For dual-mode scramjet operational applications, such a database may prove cumbersome, if not impossible, to deal with for real-time detection of the shock train leading edge.

For application to dual-mode scramjets, Rodi et al. [8] examined time-resolved pressure measurements in a scramjet inlet that was back pressured with a variable physical throat. Although the investigation was not aimed at analyzing methods for shock train leading-edge detection, the investigators found that the rms intensity of the pressure signal did indeed increase when the back pressure on the isolator was increased. In another investigation, Parrott et al. [9] monitored time-resolved pressure in the inlet, isolator, and combustor of a dual-mode scramjet. The investigators found that combustion in the scramjet combustor significantly increased the rms intensity of the wall pressure in the inlet and isolator. In addition, through spectral analysis, it was shown that combustion noise was able to propagate upstream into the isolator even though the core flow was supersonic. However, methods for shock train leading-edge detection were not explicitly examined. Le et al. [10] recently studied an isolator operating in direct-connect mode in conjunction with a dual-mode scramjet combustor. Time-resolved measurements of pressure were obtained in the isolator and it was proposed that, in addition to the magnitude of measured pressure, the rms intensity and spectral analysis could be used to detect the leading edge of a shock train in a dual-mode scramjet isolator.

Detection of the shock train leading edge would be particularly useful for operational dual-mode scramjet engine control. For example, to mitigate the risk of inlet unstart, the NASA X-43A Hyper-X research vehicle used a propulsion system controller (PSC) that monitored isolator pressure signals [11]. The purpose of the present investigation is to expand upon the work of Le et al. [10] by developing and evaluating methods by which time-resolved pressure measurements in a DMSJ isolator can be used by a PSC-type system to detect the shock train leading edge. Extending on results presented in Le et al. [10], this investigation considers and compares three methods to detect the leading edge of the shock train, using 1) a criterion based on instantaneous pressure magnitude; 2) a criterion based on the rms intensity, or standard deviation, of pressure; and 3) a power spectral analysis of the pressure signal.

This paper is organized in the following manner. First, a brief description of the facility, DMSJ, and instrumentation used in the experimental part of the investigation is presented. The time-resolved pressure measurements from the isolator of a DMSJ are then presented, which illustrate trends in the pressure magnitude and standard deviation as the equivalence ratio is varied. Next, shock train leading-edge detection methods using the defined detection criteria are examined. Shock train leading-edge detection via power spectral analysis is then conducted, and this is compared with the pressure and standard deviation results. This paper then concludes with a brief summary of results and suggestions for shock train leading-edge detection with application to PSCs for dual-mode scramjets.

II. Experimental Facility and DMSJ Model

The facility used in this study is an electrically heated, clean-air continuous-flow facility and is fully described in [12–15]. High-pressure air is provided via an oil-free compressor and desiccant dryer system. The air enters the facility at the top of a pressurized heater tank and then flows down the outer side of an annular section. The air enters the heater core at the lower end of the tank and enters a 300-kW, 14-stage electrical resistance heater, eventually reaching temperatures approaching 1200 K. This temperature enables the simulation of stagnation enthalpies equivalent to a flight Mach number near 5. After the heater, the flow enters a ceramic flow straightener and is then accelerated to Mach 2 via a two-dimensional nozzle. The isolator-combustor assembly is directly connected to the nozzle. The exit of the test section is open to the laboratory, and exhaust gases are removed from the building via an open-ended exhaust tube. The facility stagnation temperature is monitored via a type-K thermocouple, which is located in a plenum upstream of the Mach 2 nozzle. Operating conditions for the experiment are listed in Table 1.

An injection wall houses a single 10-deg unswept compression ramp that is used to introduce fuel into the flow and promote fuel–air mixing. Hydrogen is injected into the flow from the base of the ramp via a Mach 1.7 conical nozzle. All dimensions and distances are normalized here by the normal ramp height, $H = 6.35$ mm. The combustor duct inlet dimensions are $4H \times 6H$ with a 2.9-deg divergence beginning $10H$ downstream of the ramp base on the injection wall. The isolator extends $48H$ upstream of the point of fuel injection, and the exit of the combustor extends $58H$ downstream. Combustion is self-sustaining following ignition using an oxygen–hydrogen wave igniter that feeds hot combustion products into the ramp recirculation region. Both the combustor and isolator are water cooled. Further details of the combustor and isolator, along with steady state performance, are discussed in Le et al. [10]

The instrumentation is composed of three type-K thermocouples and four low-frequency pressure taps along the centerline on each of the four walls. The thermocouples were located at a depth of 0.8 mm from the flow. The low-frequency pressure taps were 1 mm in diameter and were connected to a Setra™ pressure transducer via a Scanivalve®. Time-resolved pressures were measured using high-frequency Kulite™ pressure transducers (model XTEH-10LAC-190-50A). Three of these transducers were recess mounted on the injection wall side of the isolator at the axial locations of $X = -17.8$, -27.8, and $-37.8H$ relative to the point of fuel injection (K3, K2, and K1, respectively). Three high-frequency transducers were also recess mounted on the opposite wall at the same axial locations (K6, K5, and K4, respectively). The recess mount consisted of a 3-mm-long, 1-mm-diam pressure tap with a 1-mm clearance between the tip of the high-frequency transducer and bottom of its mounting cavity. The high-frequency transducers have the ability to measure over a frequency range of 0–20 kHz. However, the recessed mount reduced

Table 1 Nominal test conditions

Parameter	Air	Fuel
Stagnation pressure, kPa	331	224–1093
Stagnation temperature, K	1010	300
Mach number[a]	2.03	1.7
Static pressure[a], kPa	41	45–221
Static temperature[a], K	600	190
Velocity[a], m/s	977	1781
Equivalence ratio	——	0.06–0.34

[a]Nozzle exit property assuming isentropic flow conditions

the frequency response of the measurement. In experimental trails, using a shock tube, Adie and Goyne [16] estimated the response of the mounted transducers to be near 5 kHz.

Because the high-frequency transducers were recess mounted, a study was conducted to investigate the possible resonance frequencies of the pressure taps. Simple harmonic resonance calculations were conducted based on the aforementioned tap geometry. Generally speaking, the resonance frequency is affected by two factors: the speed of sound and the cavity geometry. The 3-mm length of the tap allows for wavelengths of 6 mm assuming a node–node configuration for the first harmonic. Because the exact temperature of the gas inside the tap cavity was not known, average measured wall (380 K), freestream (608 K), and normal shock (957 K) temperatures were used to represent the range of possible gas temperatures. The corresponding speed of sound was calculated according to $a = (\gamma RT)^{1/2}$. The lowest resonance frequency was determined by dividing the speed of sound by the wavelength. For the wall, freestream, and normal shock temperatures, the lowest natural frequency was estimated to be 64, 78, and 101 kHz, respectively. Thus, possible resonant frequencies for the high-frequency pressure taps are significantly higher than that of the frequency of response of the Kulite pressure transducers. Resonant frequencies of the tap cavity will therefore not affect the spectral characteristics of the pressure measurements.

The high-frequency pressure signals were acquired using a 12-bit National Instruments NI-6070 data acquisition board, and the measurements were sampled at a rate of 50 kHz. Low-frequency pressure and wall temperatures were recorded using a Fluke Hydra data acquisition unit.

III. Results

Typical time-resolved pressure measurements from the DMSJ isolator are presented in Fig. 1 for an equivalence ratio, ϕ, that is first increased and then decreased with time. The pressures have been normalized by the average isolator inlet pressure, $P_{\text{ref}} = 40$ kPa, as measured by the most upstream station of the low-frequency pressure taps. The time-resolved measurements were obtained using the high-frequency pressure transducers, K1–K6, located at the three axial locations in the isolator. These results were first reported by Le et al. [10], who recognized the potential of the results for shock train leading-edge detection. Now, as an extension of that work, the pressure measurements are examined in detail and their potential is quantified.

As discussed, an increase in ϕ is expected to result in an increase in the shock train length and drive the shock train leading edge upstream through the isolator. This was reflected in the low-frequency isolator pressure measurements presented by Le et al. [10] and is confirmed by the results of Fig. 1. As ϕ is increased from its initial value at $t = 10$ s, each successive station of high-frequency pressure transducers registers the arrival of the shock train as the leading edge moves upstream. Each pair of transducers at each station registers this arrival as an increase in pressure at approximately the same time. The shock train then sweeps downstream as ϕ is decreased from its maximum value. Figure 1 further shows that, initially, for $\phi < 0.2$, a relatively steady value of P/P_{ref} is measured by each high-frequency transducer. However, at $t \sim 12$ s. and $\phi \sim 0.2$, a pressure rise is seen to occur for K3 and K6. This is an indication that the shock train has moved upstream of the combustor and into the isolator and has influenced the two most downstream high-frequency transducers in the isolator. As ϕ is increased further, a rise in pressure is sensed by K2 and K5 at $t \sim 14$ s. This indicates that the shock train has increased in length to the axial position of the transducers. This trend is seen further as ϕ is increased and a rise in pressure is seen by K1 and K4 at $t \sim 18$ s. Beyond the initial pressure rise measured by each high-frequency transducer, the pressure continues to rise as ϕ is increased further. Based on the low-frequency isolator pressure measurements of Le et al. [10], the shock train is expected to enter the facility nozzle above a combustor equivalence ratio of 0.32. This is somewhat reflected in the high-frequency pressure measurements of Fig. 1 by

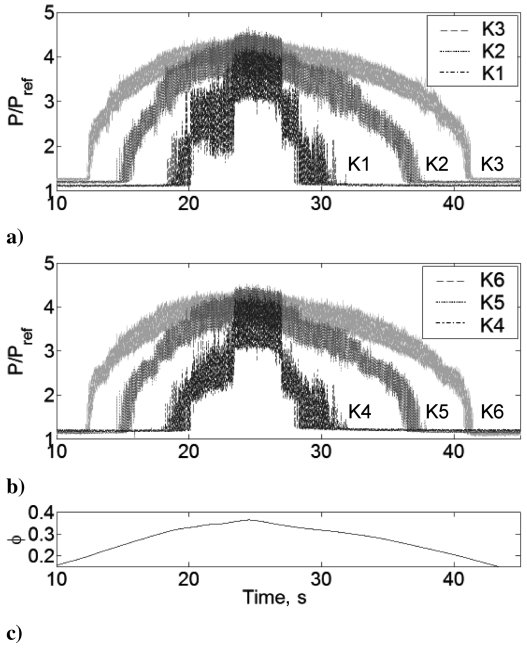

Fig. 1 Typical time-resolved measurements of wall pressure for Kulite transducers: a) K1–K3, b) K4–K6, and c) varying equivalence ratio, sampling rate of 50 kHz, $P_{\text{ref}} = 40$ kPa.

an increase in the peak-to-peak signal between $t \sim 24$ and $t \sim 27$ s. This event is discussed below. Thus, the maximum pressure ratio that can be achieved before shock-inlet interaction is approximately 4.2. At time $t \sim 25$ s, the equivalence ratio reaches a maximum and is then decreased. As can be seen in Fig. 1, the result is that the pressure measured by each high-frequency transducer decreases and the shock train recedes back into the combustor.

An examination of Fig. 1 reveals that monitoring the time-resolved pressure in the isolator would indeed seem to be an effective way of monitoring the location of the leading edge of the shock train. Based on the results and the locations of the instrumentation, the shock train leading edge is at $X = -17.8$, -27.8, and $-37.8H$ at $t \sim 12$, 14, and 18 s, respectively, as it sweeps upstream through the isolator and then is at $X = -37.8$, -27.8, and $-17.8H$ at $t \sim 31$, 37, and 41 s, respectively, as it sweeps downstream. However, for an automated monitoring system, the question still remains as to what the exact criterion for shock train detection should be. This is particularly important because the rise in pressure at $t \sim 12$ s for K6, for example, appears as a distinct change. However, the rise in pressure at $t \sim 18$ s for K4 is less distinct, and there are actually spikes that occur in the pressure signal before the main increase in pressure. Similar features are evident in K4 at $t \sim 31$ s as the shock train sweeps downstream. These features are the result of the interaction of a shock induced separation region and/or the interaction of an unsteady shock train with the high-frequency transducer. Further, comparing the pressure traces in Fig. 1 with the ϕ trace, the amount of time of interaction of the shock train leading edge with a pressure transducer would appear to be dependent on the rate of increase or decrease of ϕ. Taking these points into consideration, a criterion for shock train leading-edge detection, based on pressure magnitude, was established through trial and error. For an increasing ϕ (which is of utmost interest for inlet unstart prevention), it was found that a criterion of 150% of the steady normalized pressure level upstream of combustion influences was insensitive enough to avoid detection of pressure spikes but gave a reliable estimate of the time at which the main pressure rise actually occurred.

The results in Fig. 1 also indicate that the rms intensity of the pressure in the isolator may vary as the fuel equivalence ratio is varied and, correspondingly, as the shock train location varies. Thus, a simple statistical computation was performed to calculate the standard deviation of the pressure measurements over a running time

window. The length of the running time window was chosen to enable as much signal as possible to be analyzed over a given period while ensuring that sufficient temporal resolution was maintained and that useful information was not lost. The pressure measurements of Fig. 1 were analyzed over a running time window of 0.05 s, and the standard deviation was normalized by the average isolator inlet pressure (P_{ref}). A shorter window than this would not provide sufficient information for the statistical analysis. A slightly larger window could have been used. However, this was decided against in favor of preserving the real-time quality of the calculated parameters. In other words, a longer time window would be less useful for control schemes that require fast rise times. The results are presented in Fig. 2. As can be seen in the figure, at a low equivalence ratio ($\phi < 0.2$), the normalized standard deviation of the pressure ($\sigma_{P/P_{\text{ref}}}$) maintains a relatively low and steady value for each high-frequency transducer for $t \sim 0$–12 s at around 1% or less. However, as the equivalence ratio is increased in time, a sharp rise in $\sigma_{P/P_{\text{ref}}}$ can be seen to occur for each pair of transducers. Comparing the results with Fig. 1, the rise occurs approximately at the same time as the normalized pressure increases. As the equivalence ratio is increased further, a maximum value of $\sigma_{P/P_{\text{ref}}}$ is quickly reached in the 30–60% range and then $\sigma_{P/P_{\text{ref}}}$ decreases to a lower value. Past the maximum value, $\sigma_{P/P_{\text{ref}}}$ appears to maintain a steadier level the closer the measurement station is to the downstream end of the isolator. Some fluctuations in $\sigma_{P/P_{\text{ref}}}$ are evident in each of the pressure traces beyond the maximum value, and these may correspond to the passage of weaker shocks that are part of the shock train and are downstream of the shock train leading edge. After the peak is reached, $\sigma_{P/P_{\text{ref}}}$ tends to hover around 10–20%. However, again, this value varies somewhat with axial location. As discussed, at $\phi \sim 0.32$, the shock train enters the facility nozzle and, based on the results of Fig. 1, this is expected to occur between $t \sim 24$ and $\sim$27 s. This event is evident in the $\sigma_{P/P_{\text{ref}}}$ traces of Fig. 2, in which the level and temporal variation of $\sigma_{P/P_{\text{ref}}}$ can be seen to change at $t \sim 24$ and $\sim$27 s. Finally, as ϕ is decreased from its maximum value, similar processes in the isolator are at work. As the shock train sweeps back downstream through the isolator, $\sigma_{P/P_{\text{ref}}}$ levels eventually reach a peak and quickly fall back to the original undisturbed steady level. Reference to Fig. 1 reveals that the sharp $\sigma_{P/P_{\text{ref}}}$ fall occurs at approximately the same time the instantaneous pressure falls for each transducer.

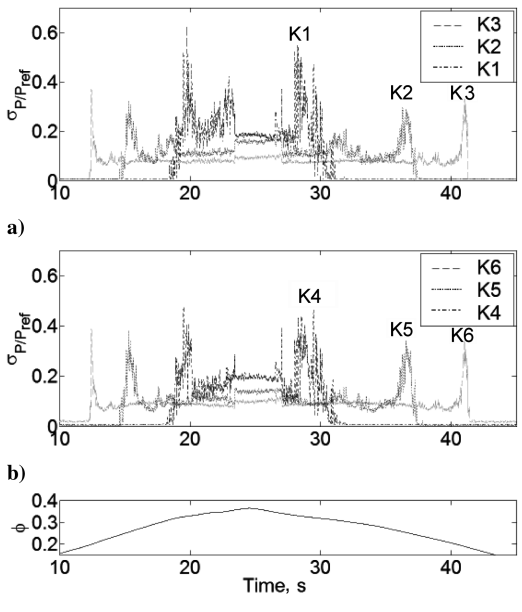

Fig. 2 Typical normalized standard deviation of the pressure measurements in Fig. 1 for Kulite transducers: a) K1–K3, b) K4–K6, and c) varying equivalence ratio.

Based on the results of Fig. 2, the monitoring of the standard deviation of the pressure signal would also appear to be a reliable way of monitoring the location of the shock train leading edge. Given that the rise in $\sigma_{P/P_{\text{ref}}}$ is even more distinct than for the instantaneous pressure magnitude, monitoring $\sigma_{P/P_{\text{ref}}}$ may be even more effective. In addition, given the change in $\sigma_{P/P_{\text{ref}}}$ that occurs when the shock train enters the facility nozzle (at $t \sim$ 24–27 s), monitoring $\sigma_{P/P_{\text{ref}}}$ in the isolator may also be an effective way of sensing inlet unstart in a real DMSJ application. As for the pressure magnitude traces, a criterion for the detection of the shock train leading edge was developed for $\sigma_{P/P_{\text{ref}}}$. For consistency with the pressure magnitude analysis, 150% of the steady value upstream of combustion influences was chosen. Through trials it was found that this criterion was also sensitive enough to detect the sharp rise in $\sigma_{P/P_{\text{ref}}}$, but insensitive enough to avoid noise and small variations in $\sigma_{P/P_{\text{ref}}}$. In addition, the maximum value of $\sigma_{P/P_{\text{ref}}}$ was chosen as another detection criterion as this value was easily determined and well defined.

It should be noted that unstart conditions during in-flight operations will be accompanied by a loss of air-mass capture. However, the facility used in this experiment does not account for this during unstart, when the shock train enters the facility nozzle. Thus, the pressure fluctuations measured during unstart in this study may not accurately reflect the actual pressure measurements that may be experienced during in-flight unstart conditions.

As discussed, three shock train leading-edge detection criteria were established: 1) 150% of the steady pressure level upstream of combustion influences, $1.5(P/P_{\text{ref}})_{\text{up}}$; 2) 150% of the steady level of normalized pressure standard deviation upstream of combustion influences, $1.5(\sigma_{P/P_{\text{ref}}})_{\text{up}}$; and 3) the maximum value of $\sigma_{P/P_{\text{ref}}}$, $(\sigma_{P/P_{\text{ref}}})_{\max}$. To examine the differences between these criteria, each was applied to an example time-resolved pressure measurement for a case of the equivalence ratio increasing with time. A sample pressure trace and corresponding standard deviation, along with the equivalence ratio, are shown in Fig. 3. The sample pressure trace and standard deviation are for one high-frequency pressure transducer, K3, with flow conditions similar to those in Table 1. The sample result is essentially the same as the traces in Figs. 1 and 2. However, the result is of particular interest because the rate of the equivalence ratio increase was lower than for Figs. 1 and 2 and, hence, the passage

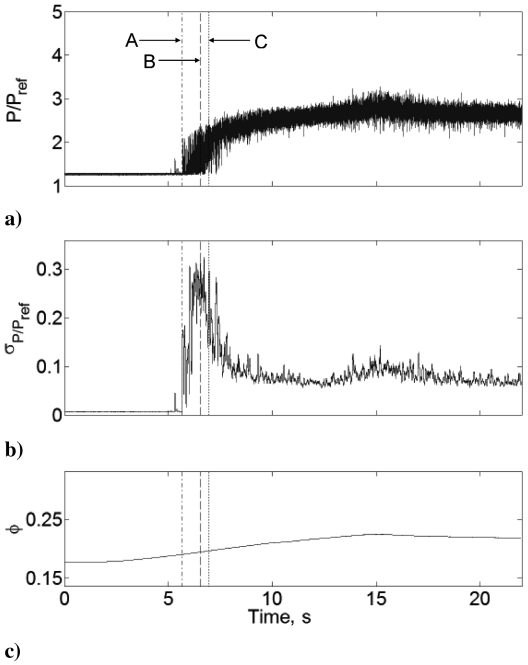

Fig. 3 Illustration of shock train detection criterion relative to a) pressure history, b) standard deviation, and c) varying equivalence ratio. Detection criteria: $A = 1.5(\sigma_{P/P_{\text{ref}}})_{\text{up}}$, $B = 1.5(P/P_{\text{ref}})_{\text{up}}$, and $C = (\sigma_{P/P_{\text{ref}}})_{\max}$.

of the shock train leading edge over the pressure transducer is a longer event. As a result, the gradual interaction of the shock train leading edge with the transducer can be observed in Fig. 3a as first a series of pressure spikes just after $t \sim 5$ s. The shock train leading edge then appears to fully reach the transducer at $t \sim 5.7$ s, with significant pressure fluctuations that decay somewhat by $t \sim 10$ s as the equivalence ratio is increased further. The location at which each detection criterion is reached is illustrated by the vertical lines in Figs. 3a–3c. As can be seen in seen in the figure, the detection criterion of $1.5(\sigma_{P/P_{\text{ref}}})$ provides the earliest method of shock train detection for this particular case.

This criterion is met by the pressure spikes that are a precursor to the full arrival of the shock train leading edge. The criterion of $1.5(\sigma_{P/P_{\text{ref}}})_{\text{up}}$ is then met by the first high-magnitude pressure spike. This is followed by the criterion of $(\sigma_{P/P_{\text{ref}}})_{\max}$ being met 1.3 s after the $1.5(\sigma_{P/P_{\text{ref}}})$ criterion was satisfied. From a scramjet combustor controls perspective, 1.3 s is a significant amount of time. Based on the present example, the criterion of $(\sigma_{P/P_{\text{ref}}})_{\max}$ would appear to the be the most conservative for detecting the shock train leading edge, whereas the criterion $1.5(\sigma_{P/P_{\text{ref}}})$ appears to be most sensitive to precursors preceding the actual leading edge.

The three shock train leading-edge detection criteria were applied to the results of Figs. 1–3, together with other available pressure traces for the case of the increasing equivalence ratio. A total of ten pressure histories were available for each high-frequency pressure transducer station at differing rates of fuel equivalence ratio increases. The equivalence ratio at which a detection criterion was satisfied was first determined and then the average equivalence ratio for the ten histories determined. The results are plotted in Fig. 4 as a function of the station's axial location. The error bars depicted represent a root sum square of a $\pm 3\%$ uncertainty in ϕ and a 95% confidence interval for the mean at each station. The figure indicates that, for an increasing ϕ, the detection criterion of $1.5(\sigma_{P/P_{\text{ref}}})$ tends to provide shock train detection at lower ϕ. The results generally mirror the trend alluded to by the example in Fig. 3, with $1.5(\sigma_{P/P_{\text{ref}}})_{\text{up}}$, $1.5(P/P_{\text{ref}})_{\text{up}}$, and $(\sigma_{P/P_{\text{ref}}})_{\max}$ generally providing shock train leading-edge detection at progressively higher equivalence ratios and later times. However, considering the experimental uncertainties and repeatability of the measurements depicted in Fig. 4, it is difficult to chose between the detection criteria, particularly at the upstream end of the isolator (more negative X/H). The error bars of Fig. 4 are expected to be not only a function of instrument error, but also of differing rates of fuel equivalence ratio increase for the data set, as well as asymmetry in the shock train at each station of transducers. However, for the generalized result of Fig. 4, it can be concluded that monitoring standard deviation of the time-resolved pressure can give as good as, if not earlier, detection of the shock train leading edge than by monitoring the magnitude of the pressure signal. Although the differences between the three methods in Fig. 4 are small in terms of ϕ, it should be kept in mind that at lower rates of change of ϕ, these differences would result in large time differences that would be significant from a controls perspective.

As discussed, spectral analysis of time-resolved pressure measurements may also prove to be an effective means of detecting the leading edge of the shock train. In fact, Le at al. [10] examined the spectral content of the data in Fig. 1 and found significant differences between the power spectra obtained from locations upstream of the shock train vs pressure spectra obtained within the shock train (at $t \sim 5$ and ~ 20 s, respectively). Upstream of the shock train, the pressure signal was mainly dc. However, within the shock train, there were high power spectral components that extended up to 4 kHz, and the spectral distribution of these components varied axially within the shock train. The spectral content of the signals of Fig. 1 and the other time-resolved pressure measurements considered above are now examined for their applicability to the detection of the shock train leading edge.

To examine the exact time at which there is a shock train leading-edge induced transition in the spectral content of the time-resolved pressure, power spectra were determined for the signals from each of the high-frequency pressure transducers using a Fourier frequency decomposition. The data of Fig. 1 were divided into 0.16-s intervals (0.32 s for a 25 kHz sampling rate), and power spectra were determined for each interval over 0–4 kHz. The power spectra were then examined to determine when significant changes occurred in the frequency content of the signals as the equivalence ratio was increased and the shock train was pushed up into the isolator. The time just before significant spectral changes occurred, together with the corresponding power spectra, are presented in Fig. 5 for the high-frequency pressure transducers, K1 and K3. The power spectra for the consecutive time interval is shown in Fig. 6. The figures show the power spectra upstream and downstream of the shock train leading edge according to the change in frequency content between two consecutive time intervals. Figure 5 illustrates the frequency content of the pressure signal just upstream of the shock train leading edge for the Kulite pressure transducer pair K1 and K3. The power spectra show that there are no significant frequency components associated

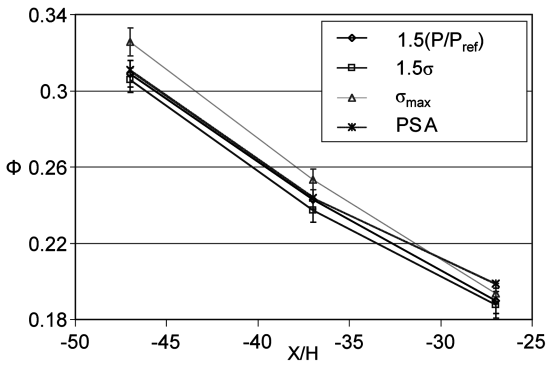

Fig. 4 Comparison of shock train detection methods

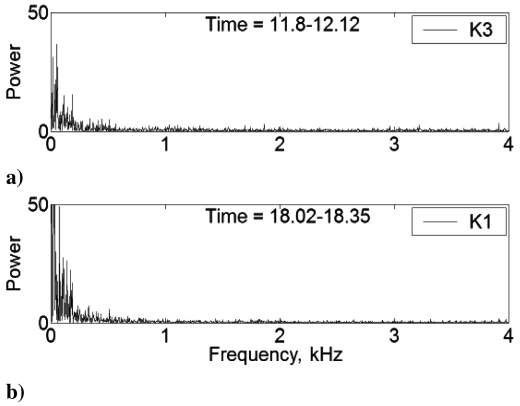

Fig. 5 Power spectra for pressure measurements in Fig. 1 upstream of the shock train leading edge: a) K3, and b) K1.

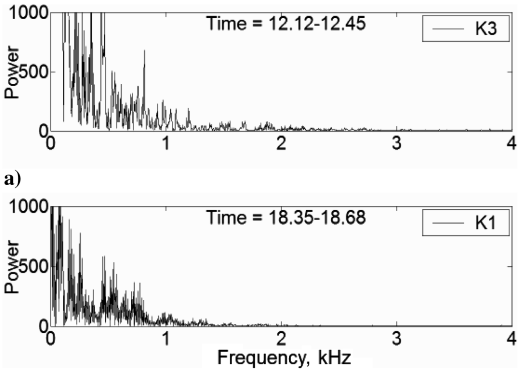

Fig. 6 Power spectra for pressure measurements in Fig. 1 downstream of the shock train leading edge: a) K3, and b) K1.

with the pressure signal upstream of combustion influences for each high-frequency transducer. Similar results are seen for other pressure transducers. The power spectra shown in the consecutive time interval, Fig. 6, show a significant increase in the frequency content.

As may be expected from the data in Fig. 1, the time at which this change in the power spectra occurs is the same as for each pair of transducers at each station, but it occurs at a progressively later time the further upstream the station is located. The time at which this change occurs at each station is also consistent with the data in Fig. 1. The power spectra also indicate that there may be dominant frequency components associated with this portion of the pressure signal. There are peaks in the power spectra below 1 kHz that are evident for the two most upstream stations (e.g., Fig. 6b). The power spectra for Kulite pressure transducers downstream of the shock train leading edge all exhibit similar increased frequency content as observed initially by Le et al. [10]. There is a broad range of frequency content of varying power associated with this region of the pressure signal, which was found to be typical of the pressure signal well downstream of the shock train leading edge. Interestingly, there are changes in the power spectra profile with the station axial location. These results indicate that a change in the frequency components shown in the power spectra is directly related to the influence of the shock train.

These results indicate that a change in the frequency components of the power spectra is directly related to the influence and location of the shock train. Before shock train interaction, there are no significant frequency components beyond about 0.2 kHz. However, frequency components of varying power are observed at the leading edge of the shock train and downstream of the leading edge. Thus, spectral content can be used to detect the leading edge of the shock train. To compare this method with the pressure magnitude and rms intensity criteria developed, the time at which the power spectra first changed in Fig. 5 was noted and the corresponding equivalence ratio determined. The data are compared in Fig. 4. Comparison of the power spectral analysis results reveals that the power spectra are indeed well correlated with changes in the magnitude of the measured pressure and, apart from the most upstream station, the method detects the shock train leading edge with the same sensitivity as the $1.5(P/P_{\text{ref}})_{\text{up}}$ criterion. More important, however, the power spectral analysis method does not yield shock train leading-edge detection at lower equivalence ratios or, equivalently, at earlier times than any of the other criteria developed.

Summarizing the results of this investigation, instantaneous pressure levels, pressure rms intensity, and pressure signal spectral analysis are all suitable for use in detecting the leading edge of the shock train. For a particular PSC application, 150% of the normalized pressure standard deviation level upstream of combustion influences would tend to provide the earliest indication of the approach of the shock train leading edge as it sweeps upstream toward a certain point in the isolator. However, monitoring the peak in the normalized pressure standard deviation would tend to be the most conservative method of determining if the shock train leading edge has actually reached that point. The time between these two criteria being met could be on the order of seconds or even more, depending on the speed of the shock train leading edge. Although spectral analysis of the time-resolved pressure can be used to locate the shock train, it is computationally more intensive. Based on the present results, it would appear less suitable for real-time PSC applications than the pressure magnitude and rms intensity monitoring. Further, pressure magnitude in the isolator is affected by vehicle and flight conditions and by inlet geometry that may be variable. In addition, the time at which the maximum in normalized pressure standard deviation occurs is only known a posteriori. Therefore, monitoring rms intensity increases may be the best way of determining the shock train leading-edge location in the isolator for an operational application.

Having reached this conclusion, there are some caveats that should be addressed. Although determined after substantial consideration, the detection levels or, equivalently, the criteria factors for the pressure magnitude and pressure rms intensity criteria are somewhat arbitrary. For the present study, the use of a higher or lower criteria factors would lead to a later or earlier detection of the shock train leading edge, respectively. The use of a lower criteria factor would increase the risk of shock detection based purely on signal noise. But, nevertheless, further experiments, especially those involving shock train visualization in the isolator, would be useful to determine the optimal detection criteria and the exact location of the shock train leading edge when the criteria was met. The optimal size of the running time window used to determine the pressure standard deviation also should be examined. A smaller or larger running time could be used. However, it is important to remove the effect of noise in the pressure signature without deterioration of the rise time necessary for control scheme techniques. In addition, the most appropriate criteria factor, or even criteria, may also be application specific. For instance, for applications involving a shock train that moves upstream into the isolator at high speed, the differences observed between the detection criteria may not be as well defined as they are in the present study. Such a situation may arise if the rate of the fuel equivalence ratio increase is very high or if there is a sudden change in the combustor induced pressure rise or combustor geometry.

Other situations may yield additional complications that should be examined. If a particular application involves an inlet generated shock train that is captured by the isolator, then the isolator flowfield will be somewhat more complicated than a simple combustor pressure induced shock train. If the inlet shock system does not lead to boundary-layer separation in the isolator, then the findings of the present study remained largely unaltered. This is because the pressure signal associated with the isolator shock train leading edge is dominated by the boundary-layer separation process. However, if boundary-layer separation is induced by the inlet shock then a question remains as to whether a control system could be designed to decipher between an inlet shock induced separation and that induced by the isolator shock train leading edge. Further experimental study can only answer this question.

Finally, spectral analysis may prove more useful if time-resolved pressure measurements can be made in the combustor and specific combustion induced frequency components identified. If these specific components travel upstream through the isolator via the shock train or subsonic separated flowpaths, spectral detection of the shock train leading edge may be more straightforward because filtering techniques could be used rather than Fourier decomposition methods. Such a scheme may also aid in the identification the shock train leading edge when the isolator flowfield is complicated by a captured inlet shock system.

IV. Conclusions

Time-resolved measurements of pressure in the isolator of a direct-connect dual-mode scramjet were analyzed to examine the potential of using such measurements in shock train leading-edge detection. Methods that would suit PSC-type algorithms were examined and it was found that instantaneous pressure levels, pressure rms intensity, and pressure signal spectral analysis were all capable of locating the leading edge of the shock train as the shock train was pushed out of the scramjet combustor and up through the isolator. Each of these methods would thus be suitable candidates for control schemes that are aimed at preventing combustor–inlet interaction. Considering practical applications, monitoring the standard deviation of wall pressure, or rms intensity, appears to be the best method to determine the location of the shock train leading edge. In the present study, 150% of the normalized pressure standard deviation level upstream of combustion influences worked well as a criteria for the earliest indication of the approach of the shock train leading edge.

Acknowledgments

The authors appreciate the financial support of the National Institute of Aerospace under NIA project 3002-VA. A.H. Auslender of NASA Langley Research Center served as technical monitor. Discussions with K.E. Rock of NASA Langley Research Center are also appreciated. Some testing was also supported by NASA under

grant NAG-1-02019 with C.R. McClinton and D.E. Reubush of NASA Langley Research Center as technical monitors. The authors would also like to acknowledge J.C. McDaniel for his input. In addition, the authors appreciate the contribution of P.F. Adie to the isolator engineering design.

References

[1] Billig, F. S., "Research on Supersonic Combustion," *Journal of Propulsion and Power*, Vol. 9, No. 4, 1993, pp. 499–514.

[2] Cockrell, C. E., Jr., Auslender, A. H., Guy, R. W., McClinton, C. R., and Welch, S. S., "Technology Roadmap for Dual-Mode Scramjet Propulsion to Support Space-Access Vision Vehicle Development," AIAA Paper 2002-5188, 2002.

[3] Heiser, W. H., and Pratt, D. T., *Hypersonic Airbreathing Propulsion*, AIAA Education Series, AIAA, Washington, D.C., 1994.

[4] Matsuo, K., Mochizuki, H., Miyazato, Y., and Gohya, M., "Oscillatory Characteristics of a Pseudo-Shock Wave in Rectangular Straight Duct," *JSME International Journal, Series B (Fluids and Thermal Engineering)*, Vol. 36, No. 2, 1993, pp. 222–229.

[5] Hamed, A., and Shang, J. S., "Survey of Validation Data Base for Shockwave Boundary-Layer Interactions in Supersonic Inlets," *Journal of Propulsion and Power*, Vol. 7, No. 4, 1991, pp. 617–625.

[6] Carroll, B. F., and Dutton, J. C., "Turbulence Phenomena in a Multiple Normal Shock Wave/Turbulent Boundary-Layer Interaction," *AIAA Journal*, Vol. 30, No. 1, 1992, pp. 43–48.

[7] Sajben, M., Donovan, J. F., and Morris, M. J., "Experimental Investigation of Terminal Shock Sensors for Mixed-Compression Inlets," *Journal of Propulsion and Power*, Vol. 8, No. 1, 1992, pp. 168–174.

[8] Rodi, P. E., Emami, S., and Trexler, C. A., "Unsteady Pressure Behavior in a Ramjet/Scramjet Inlet," *Journal of Propulsion and Power*, Vol. 12, No. 3, 1996, pp. 486–493.

[9] Parrott, T. L., Jones, M. G., and Thurlow, E. M., "Unsteady Pressure Loads in a Generic High-Speed Engine Model," NASA TP 3189, 1992.

[10] Le, D. B., Goyne, C. P., Krauss, R. H., and McDaniel, J. C., "Experimental Study of a Dual-Mode Scramjet Isolator," AIAA Paper 2005-0023, 2005.

[11] Jones, P. T., and Baumann, E., "Evaluation of the X-43A Scramjet Engine Controller Performance by Monte Carlo Technique," AIAA Paper 2003-5192, 2003.

[12] Goyne, C. P., Rodriguez, C. G., Krauss, R. H., McDaniel, J. C., and McClinton, C. R., "Experimental and Numerical Study of a Dual-Mode Scramjet Combustor," *Journal of Propulsion and Power*, Vol. 22, No. 3, 2006, pp. 481–489.

[13] Krauss, R. H., and McDaniel, J. C., "A Clean Air Continuous Flow Propulsion Facility," AIAA Paper 92-3912, 1988.

[14] Krauss, R. H., McDaniel, J. C., Jr., Scott, J. E., Jr., Whitehurst, R. B., III, Sega, C., Mahoney, G. T., and Childers, J. M., "Unique, Clean-Air, Continuous-Flow, High-Stagnation-Temperature Facility for Supersonic Combustion Research," AIAA Paper 88-3059, 1988.

[15] Goyne, C. P., McDaniel, J. C., Krauss, R. H., and Whitehurst, W. B., "Test Gas Vitiation Effects in a Dual-Mode Scramjet Combustor," *Journal of Propulsion and Power*, Vol. 23, No. 3, 2007, pp. 559–565. doi:10.2514/1.24663

[16] Adie, P. F., and Goyne, C. P., "An Investigation of Pressure Tap Geometries and Their Relationship to Transducer Rise Time," *AIAA Region I-MA Student Conference*, AIAA, Reston, VA, 2004.

L. Maurice
Associate Editor